J Math Chem (2014) 52:2234–2258
DOI 10.1007/s10910-014-0382-5

ORIGINAL PAPER

Quadratic autocatalysis with non-linear decay

Ahmed Hussein Msmali · Mark I. Nelson · Maureen P. Edwards

Received: 13 January 2014 / Accepted: 23 June 2014 / Published online: 5 July 2014

Abstract We provide a detailed, and thorough, investigation into the concentration multiplicity and dynamic stability of a prototype non-linear chemical mechanism: quadratic autocatalysis subject to non-linear decay in a continuously stirred tank reactor. This model was previously investigated in the literature using numerical path-following techniques. The contribution of this study is the application of singularity theory and degenerate Hopf-bifurcation theory to obtain analytical representations of many of the features of interest in this system. In particular, we use these presentations to identify critical values of an unfolding parameter below which specified phenomenon are no longer exhibited.

Keywords Autocatalysis · Flow reactor · Hopf bifurcation · Singularity theory

Mathematics Subject Classification 80A32 · 92E20

1 Introduction

Quadratic autocatalysis and the closely related cubic autocatalysis have been widely investigated as prototype non-linear chemical kinetic schemes [1–3]. Although conceptually simple, these schemes qualitatively capture the behaviour of a range of chemical systems [3, p. 9]. In particular quadratic autocatalysis has proven to be a simple prototype for more complicated kinetic structures possessed by large families of cooperative biochemical systems, inorganic solution-phase oscillatory reactions, surface catalysis and gas phase branched-chain reactions.

A. H. Msmali · M. I. Nelson (✉) · M. P. Edwards
School of Mathematics and Applied Statistics, University of Wollongong,
Wollongong, NSW 2522, Australia
e-mail: mnelson@uow.edu.au

The steady-state multiplicity and dynamic behaviour of isothermal autocatalytic reactions in a continuously stirred tank reactor was first investigate by Lin [4,5]. Lin considered the reaction mechanism

$$A + B \rightarrow (1 + r)B, \quad \text{rate} = k_1 a^m b^n. \tag{1}$$

The cases $r = 1$ and $r \neq 1$ were considered in [4] and [5] respectively.

The study of quadratic (and cubic) autocatalytic schemes was popularised by Gray and Scott. In [6] they introduced the two-step reaction scheme

$$A + B \rightarrow 2B, \quad \text{rate} = k_1 ab, \tag{2}$$

$$B \rightarrow C, \quad \text{rate} = k_2 b. \tag{3}$$

The first reaction represents a quadratic autocatalytic reaction, with stoichiometry $A \rightarrow B$, whereas the second reaction represents the decay of the autocatalytic species (B). The decay of the catalyst may be the result of further chemical reaction (homogeneous or heterogenous), be due to poisoning or to physical degradation.

For gas-phase reactions the autocatalytic reaction (2) is a prototype for rate limiting steps where a stable reactant reacts with one radical to give two radicals such as $O_2 + H \rightarrow OH + O$. In such systems the deactivation of the autocatalyst occurs through a radical termination reaction on the reactor surface and the linear decay rate (3) is replaced by the non-linear decay rate

$$B \rightarrow C, \quad \text{rate} = k_2 b/(1 + rb). \tag{4}$$

The use of the system (2) and (4) to model isothermal branched-chain reactions was considered in [7–9]. The application to the isothermal oxidation of carbon monoxide is discussed in [8] and to oxidation of hydrogen in [8,9]. The decay step (4) can also model autocatalyst deactivation via an enzyme-catalysed process.

Merkin et al. [7,8] concentrated their analysis on the case when there is no autocatalyst in the feed stream in the reactor and derived asymptotic expressions for the occurrence of sustained oscillatory behaviour. In [7] the nature of the stationary steady-state solutions and their local stability was investigated. In [8] the nature of the limit cycles was investigated.

Brindley et al. [9] presented a detailed, and thorough, numerical investigation of the static and dynamic behaviour of the scheme (2) and (4) based on the use of numerical path-following techniques.

The main purpose of this paper is to show that path following schemes are not required to construct the bifurcation surface of the system formed by reaction steps (2) and (4). Instead these curves are parameterised analytically through the application of singularity theory and degenerate Hopf bifurcation theory. These parameterisation are used to establish some exact criterion for the effect of the saturation constant (ρ) upon static multiplicity and uniqueness. We also establish some additional results for this system which have not appeared in the literature previously.

The techniques of singularity theory and degenerate Hopf bifurcation theory were not widely known at the time of the investigations [7–9]. Furthermore, it may not have

even been practical to apply them as many of the calculations required are greatly eased by the use of a symbolic manipulation package. Where appropriate we outline the results we use from singularity theory and degenerate Hopf bifurcation theory. For a more detailed discussion for these results, in particular their application, we refer to Ajbar and Alhumaizi [10].

2 Model equations

2.1 Dimensional model

The model equations for a chemical process governed by quadratic autocatalysis with catalyst decay are

$$V\frac{da_1}{dt} = q(a_0 - a_1) - Vk_1a_1b_1, \tag{5}$$

$$V\frac{db_1}{dt} = q(b_0 - b_1) + Vk_1a_1b_1 - \frac{Vk_2b_1}{(1 + rb_1)}. \tag{6}$$

In Eqs. (5)–(6), a_0 is the reactant concentration in the feed (mol m^{-3}), a_1 is the reactant concentration (mol m^{-3}), b_0 is the autocatalyst concentration in the feed (mol m^{-3}), b_1 is the autocatalyst concentration (mol m^{-3}), k_1 is the rate constant for the autocatalytic step (m^3 mol^{-1} s^{-1}), k_2 is the decay rate (s^{-1}), q is the flow rate through the reactor (m^3 s^{-1}), r is the surface saturation term (m^3 mol^{-1}), t is the time (s) and V is the volume of the reactor (m^3).

The main experimental control parameter in Eqs. (5)–(6) is the residence time t

$$t = \frac{q}{V}. \tag{7}$$

2.2 Dimensionless model

To non-dimensionalise the Eqs. (5)–(6) we introduce the variables groups: $\alpha_1 = a_1/a_0$, $\beta_1 = b_1/a_0$, and $t^* = k_1a_0t$. The system (5)–(6) can be written in the form

$$\frac{d\alpha_1}{dt^*} = \frac{1 - \alpha_1}{\tau} - \alpha_1\beta_1, \tag{8}$$

$$\frac{d\beta_1}{dt^*} = \frac{\beta_0 - \beta_1}{\tau} + \alpha_1\beta_1 - \frac{\kappa_2\beta_1}{1 + \rho\beta_1}, \tag{9}$$

where the parameter groups are: the dimensionless concentration of the autocatalytic species in the feed, $\beta_0 = b_0/a_0$; the dimensionless decay-rate, $\kappa_2 = k_2/(k_1a_0)$; the dimensionless saturation term, $\rho = ra_0$; and the dimensionless residence time, $\tau = Vk_1a_0/q$. For numerical calculations we follow [9] and consider the case $\rho = 10$.

Merkin et al. [7,8] concentrated on the case when there is no autocatalyst in the feed stream ($\beta_0 = 0$). and for the asymptotic limit $\kappa_2 = k_2/(k_1a_0) \ll 1$. The case when

there is autocatalyst in the feed ($\beta > 0$) was investigated numerically in [9]. Indeed, it was previously thought the condition $\beta_0 = 0$ was *required* for analytic progress in understanding the system (8) and (9). We demonstrate that this is not the case.

In the Appendix we show that the region

$$0 \leq \alpha_1 \leq 1,$$
$$0 \leq \alpha_1 + \beta_1 \leq 1 + \beta_0$$

is both (positively) invariant and exponentially attracting for any solution with physically meaningful initial conditions outside it.

3 Results: static multiplicity

The steady-state solutions are given by

$$\beta_1 = \frac{1 - \alpha_1}{\tau \alpha_1} \tag{10}$$

where α_1 is a root of the singularity function

$$G = (\tau - \rho)\,\tau\alpha_1^3 - \left\{(\beta_0 + 1 + \kappa_2)\,\tau^2 + [(-2 - \beta_0)\,\rho + 1]\,\tau - \rho\right\}\alpha_1{}^2 + \left\{\kappa_2\tau^2 + [1 - (\beta_0 + 1)\,\rho]\,\tau - 2\rho\right\}\alpha_1 + \rho. \tag{11}$$

Equations (10) and (11) were originally derived in [7]. Note that when there is no autocatalyst in the inflow ($\beta_0 = 0$) then the 'washout solution' $\alpha_1 = 1$, corresponding to $\beta_1 = 0$, is a root of the singularity equation (11). The latter then reduces to a quadratic equation [7].

What is new here is the application of singularity theory to investigate the behaviour of Eq. (11).

3.1 The cusp singularity

Theorem 3.1 (Cusp singularity) *Suppose that at the point* $(\mu, x, \alpha) = (\mu, x_0, \alpha_0)$ *the singularity function* $G(\mu, x, \alpha)$ *satisfies the equations*

$$G = G_x = G_{xx} = 0, \tag{12}$$
$$G_\mu \cdot G_{xxx} \neq 0. \tag{13}$$

Then a cusp singularity, or hysteresis point, occurs at the point (μ, x_0, α_0) [10, p. 33].

3.1.1 Parameterising the cusp locus

In this section we obtain a parameterisation of the cusp locus. This is used to show that there is no cusp singularity if the saturation constant is sufficiently low ($\rho < 4$).

Applying conditions (12) to Eq. (11) we obtain

$$\kappa_2 = \frac{[(\alpha_1 - \beta_0 - 1)\tau\alpha_1 + 1 - \alpha_1)]\,[(\rho - \tau)\,\alpha_1 - \rho]}{\tau^2\alpha_1\,(1 - \alpha_1)}, \tag{14}$$

$$\beta_0 = -\frac{(1 - \alpha_1)^2\left[(\tau - \rho)\,\tau{\alpha_1}^2 + \rho\right]}{\tau^2{\alpha_1}^2}, \tag{15}$$

$$\alpha_1 = \sqrt[3]{\frac{\rho}{\tau\,(\rho - \tau)}}. \tag{16}$$

The expression (15) can be substituted into (14) to obtain, for fixed saturation constant ρ, a one-parameter parameterisation of the cusp locus.

A necessary condition for Eq. (16) to be physically meaningful is that $0 < \tau < \rho$. Furthermore, we must also have $\alpha_1 \leq 1$. From (16) this gives

$$\tau^2 - \rho\tau + \rho \leq 0. \tag{17}$$

Inequality (17) can not hold if $0 < \tau < 1$. Thus a necessary condition for a cusp singularity is that $1 < \tau < \rho$. Furthermore, from the inequality (17) we require

$$\frac{\rho - \sqrt{\rho(\rho - 4)}}{2} \leq \tau \leq \frac{\rho + \sqrt{\rho(\rho - 4)}}{2}. \tag{18}$$

Equation (18) shows that there is no cusp singularity when $0 < \rho < 4$.

It is useful when drawing the cusp locus to know the conditions for which the value of β_0 at the cusp singularity is zero. After some algebra we find that

$$\alpha(\beta = 0) = 1, \tag{19}$$

$$\rho(\beta_0 = 0) = \frac{\tau^2}{\tau - 1}, \tag{20}$$

$$\kappa_2(\beta_0 = 0) = \frac{\tau - 1}{\tau}, \tag{21}$$

$$\tau\,(\beta_0 = 0) = \frac{\rho \pm \sqrt{\rho(\rho - 4)}}{2}. \tag{22}$$

When $\rho = 10$ we find from Eq. (22) that $\tau_\pm = 5 \pm \sqrt{15}$. The corresponding values for the dimensionless decay rate are $\kappa_{2_-} = \left(5 - \sqrt{15}\right)/10 \approx 0.113$ and $\kappa_{2_+} = \left(5 + \sqrt{15}\right)/10 \approx .887$.

Thus there is no cusp singularity when $\kappa_2 < \kappa_{2_-}$. This critical value for the decay rate was found to be $1/9 \approx 0.111$ using path-following methods [9, p. 484].

3.1.2 The non-degeneracy conditions

The non-degeneracy conditions are $G_\mu \neq 0$ and $G_{xxx} \neq 0$.

Table 1 Location of points along the isola singularity where the non-degeneracy condition $G_{\alpha_1\alpha_1} \neq 0$ fails

α_1	0.75123	0.8603
τ	3.81143	8.049
β_0	0.02499	0.0006
κ_2	1.05467	0.889

These are also points also the cusp singularity where the non-degeneracy condition $G_\tau \neq 0$ fails. Parameter value: $\rho = 10$

The first non-degeneracy condition corresponds to points which are intersection points of the cusp and isola locii. The parameterisation for such points is discussed in Sect. 3.2.2. Their location when $\rho = 10$ is given in Table 1. Observe that there is a degenerate point at $\kappa_2 = 1.05467$, above which the cusp singularity does not occur. Using path-following methods it was identified in [9, p. 485] that the cusp singularity is not possible when $\kappa_2 > 1.056$.

After some algebra we find that the second non-degeneracy condition fails when

$$(\tau\rho, \alpha_1, \kappa_2, \beta_0) = (0, 0, \alpha_1, \kappa_2, \beta_0)\,. \tag{23}$$

This possibility can be excluded for several reasons, such as the requirement that $\tau = \rho = 0$ when the model assumes $\rho > 0$.

3.1.3 Plotting the cusp curve

The cusp curve is shown in Fig. 1a. Figure 1b blows up Fig. 1a to more clearly show the behavior near the point $(\kappa_2, \beta_0) = (0.887, 0)$.

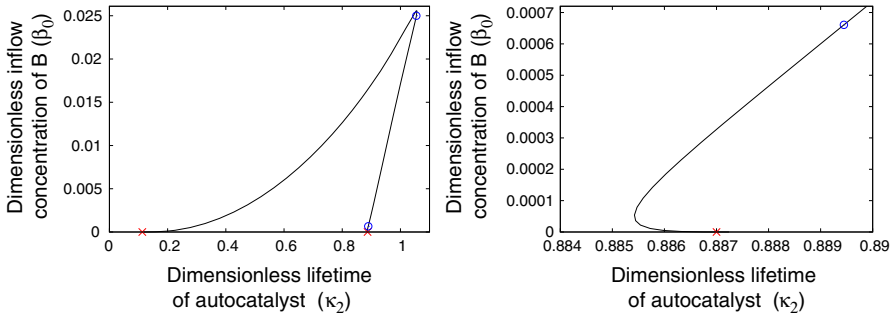

Fig. 1 The cusp singularity in the secondary bifurcation parameter plane. Parameter value: $\rho = 10$. The *red crosses* denote the crossing points (κ_2, β_0)=(0.113, 0) and (0.887, 0). The *circles* denote points where the non-degeneracy condition $G_\tau \neq 0$ fails. These are: $(\kappa_2, \beta_0) = (0.889, 0.66 \times 10^{-3})$ and (1.055, 0.025) (Color figure online)

3.2 The isola singularity

Theorem 3.2 (Isola singularity) *Suppose that at the point* $(\mu, x, \alpha) = (\mu, x_0, \alpha_0)$ *the singularity function* $G(\mu, x, \alpha)$ *satisfied the equations*

$$\begin{aligned} &G = G_x = G_\mu = 0, \\ &G_{xx} \neq 0, \\ &G_{xx} G_{\mu\mu} - (G_{x\mu})^2 \neq 0. \end{aligned} \tag{24}$$

Then an isola singularity occurs at the point (μ, x_0, α_0) [10, p. 33].

3.2.1 Parameterising the isola locus

In this section we obtain a parameterisation of the isola locus. This is used to show that there is no isola singularity if the autocatalyst feed concentration is sufficiently high ($\beta_0 > 1/8$) or the saturation constant is sufficiently low ($\rho < 8/(1 - 8\beta_0)\,,\ \beta < 1/8$). In particular, there can be no isola singularity if $\rho < 8$.

Applying the conditions (24) to Eq. (11) we obtain

$$\tau = -\frac{\rho\,(1-\alpha_1)}{\alpha_1\left(\rho{\alpha_1}^2 - \rho\alpha_1 + 1\right)}, \tag{25}$$

$$\beta_0 = \alpha_1\,(3 - 2\alpha_1) - \frac{1+\rho}{\rho}, \tag{26}$$

$$\kappa_2 = \rho\,(1-\alpha_1)\,{\alpha_1}^3. \tag{27}$$

It is sometimes useful to rewrite Eq. (25) as

$$\rho = \frac{\tau\alpha_1}{(1-\alpha_1)\left(\tau{\alpha_1}^2 - 1\right)}. \tag{28}$$

From Eq. (26) the reactant concentration (α_1) along the isola singularity locus is given by

$$\alpha_1 = \frac{3 \pm \sqrt{1 - 8\,(\beta_0 + 1/\rho)}}{4}. \tag{29}$$

It follows that there is no isola singularity when

$$\rho\,(1 - 8\beta_0) < 8. \tag{30}$$

Hence there can not be an isola singularity if either the autocatalytic feed concentration is greater than a critical value ($\beta_{0,\mathrm{cr}} = 1/8$) or if the saturation constant is sufficiently low. Indeed, there can be no isola singularity, regardless of the feed concentration, if the saturation constant is smaller than a critical value ($\rho_{\mathrm{cr}} = 8$).

It is useful when drawing the isola locus to know the conditions for which the value of β_0 on the isola singularity is zero. These are

$$\alpha_1\left(\beta_0=0\right)=\frac{3\pm\sqrt{1-\frac{8}{\rho}}}{4}, \tag{31}$$

$$\kappa_2(\beta_0=0)=\frac{{\alpha_1}^3}{2\alpha_1-1}, \tag{32}$$

$$\tau\left(\beta=0\right)=\frac{2}{\alpha\left(1-\alpha\right)}. \tag{33}$$

Equation (31) reveals that there are no intersection points along the line $\beta_0 = 0$ if $\rho < 8$.

When $\rho = 10$ we find from Eq. (31) that the isola locus crosses the line $\beta = 0$ when $\alpha_{1_\pm} = \left(15 \pm \sqrt{5}\right)/20$. The corresponding values for the dimensionless decay rate are $\kappa_{2_-} = \left(73 + \sqrt{5}\right)/80 \approx 0.940$ and $\kappa_{2_+} = \left(73 - \sqrt{5}\right)/80 \approx 0.884$.

3.2.2 The non-degeneracy conditions

The non-degeneracy conditions are $G_{xx} \neq 0$ and $G_{xx}G_{\mu\mu} - \left(G_{x\mu}\right)^2 \neq 0$.

At points where the first non-degeneracy condition is violated the cusp and isola curves intersect. Substituting (25)–(27) into the non-degeneracy condition and solving for the dimensionless saturation constant we have

$$\rho = 0, \tag{34}$$

$$\rho=\frac{1\pm\sqrt{4\,\alpha_1-3}}{2\left(1-\alpha_1\right)^2\alpha_1}. \tag{35}$$

The physically meaningful solutions of the system comprising Eqs. (25)–(27) and (35) when $\rho = 10$ are given in Table 1.

Now we consider where the second non-degeneracy condition, $G_{xx}G_{\mu\mu} - (G_{x\mu})^2 \neq 0$, is violated. Let $H = G_{\alpha_1\alpha_1}G_{\tau\tau} - (G_{\alpha_1\tau})^2$. Substituting the isola singularity expressions (25–27) into H and simplifying we obtain

$$\begin{aligned}H=&\left(\alpha_1+3\right)\left(1-\alpha_1\right)^3{\alpha_1}^2\rho^2+2\alpha_1\left(1-\alpha_1\right)\left({\alpha_1}^2-2\alpha_1-1\right)\rho\\&+\alpha_1\left(2-\alpha_1\right)+3.\end{aligned} \tag{36}$$

The physically meaningful solutions of the system comprising Eqs. (25)–(27) and (36) are given in Table 2.

3.2.3 Plotting the isola curve

The isola curve is shown in Fig. 2.

Table 2 Location of points along the isola singularity where the non-degeneracy condition $G_{\alpha_1,\alpha_1} G_{\tau,\tau} - (G_{\alpha_,\tau})^2 \neq 0$ fails

α_1	0.747	0.860
τ	3.80621	8.062
β_0	0.02498	0.0006
κ_2	1.05460	0.889

Parameter value: $\rho = 10$

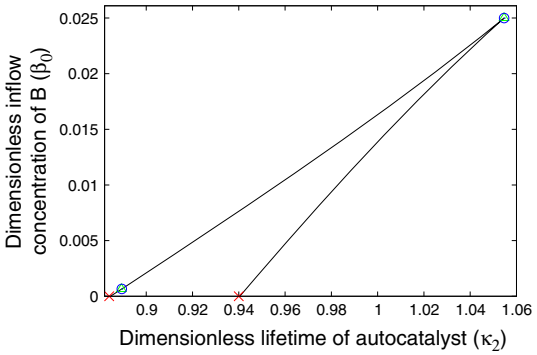

Fig. 2 The isola singularity in the secondary bifurcation parameter plane. Parameter value: $\rho = 10$. The crossing points are (κ_2, β_0)=(0.884, 0) and (0.940, 0). The *circle* and *triangle points* are $(\kappa_2, \beta_0) = (0.889, 0.6 \times 10^{-3})$ and (1.055, 0.025). These represent the points where the non-degeneracy condition $G_{xx} \neq 0$ and $G_{xx} G_{\mu\mu} - (G_{x\mu})^2 \neq 0$ fail respectively. (To graphical accuracy these points are identical)

3.2.4 Static multiplicity: combining the cusp and isola singularity locii

Figure 3 shows the static bifurcation diagram, which is the union of the cusp and isola singularity curves. These curves split the secondary bifurcation plane into five regions. Thus the model (8) and (9) has five generic static steady-state diagrams, i.e. five types of response diagram showing the dimensionless reactant concentration (α_1) as a function of the dimensionless residence time (τ). Figure 3b, c blow up Fig. 3a to more clearly show the location of smaller regions.

Region *a* represents a unique steady-state diagram, see Fig. 20a, region *b* represents a breaking wave steady-state diagram, see Fig. 13a, region *c* represents an isola steady-state diagram, see Fig. 14a, region *d* represents a mushroom steady-state diagram, see Fig. 19a, and region *e* represents an isola with breaking wave steady-state diagram, see Fig. 16. Note that the last type does not occur without at least one Hopf bifurcation.

Figure 3 was previously obtained using path following methods [9, Figure 1.]. Here it is plotted using the parametric representation of the singularity curves. Using our representations it is much easier to investigate how the static bifurcation diagram changes as a function of the saturation parameter (ρ).

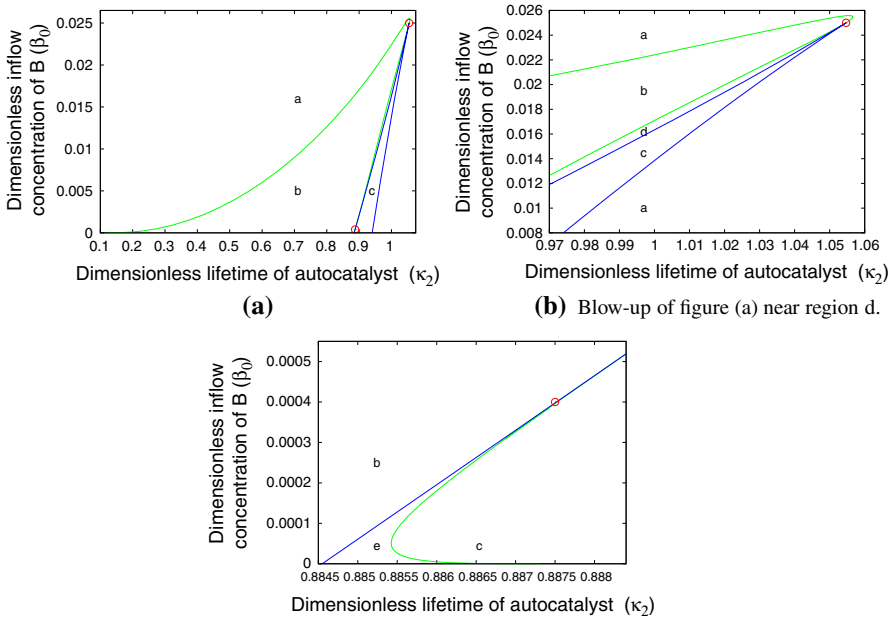

(a)

(b) Blow-up of figure (a) near region d.

(c) Blow-up of figure (a) near region e.

Fig. 3 Static bifurcation diagram showing the cusp (*green curve*) and isola (*blue curve*) singularities. The *red circle* points are the intersection points between cusp and isola curve located at: $(\kappa_2, \beta_0) = (0.8875, 0.0004)$ and $(\kappa_2, \beta_0) = (1.0546, 0.0249)$. Parameter value: $\rho = 10$ (Color figure online)

4 Results: dynamic multiplicity

4.1 The Hopf bifurcation theorem

A Hopf bifurcation [11, chapter 1], [12, chapter 5] occurs when a pair of complex eigenvalues crosses the imaginary axis. Associated with this is the formation (or destruction) of a limit cycle.

Theorem 4.1 (Hopf bifurcation theorem) *Suppose that a two-dimensional system*

$$\frac{dx}{dt} = f(x, \mu), \quad x \in \Re^2, \ \mu \in \Re, \tag{37}$$

with $f \in C^2$ *has a steady-state solution* $x(\mu)$ *with imaginary eigenvalues*

$$\lambda_{1,2} = \mu(\mu) \pm i w(\mu)$$

which are purely imaginary at $\mu = \mu_0$, *i.e.* $\mu(\mu_0) = 0$ *and* $w(\mu_0) > w_0$. *Let the following non-degeneracy conditions be satisfied:*

(1) The derivative of the real part of the eigenvalues with respect to the bifurcation parameter, μ, is non-zero, i.e.

$$\frac{d}{d\mu} Re\lambda_{1,2}(\mu)\bigg|_{\mu=0} \neq 0.$$

(2) $l_1(0) \neq 0$, where l_1 is known as the first Lyapunov coefficient.

Then it can be shown that a unique limit cycle bifurcate from the steady-state solution at the Hopf bifurcation point $(x, \mu) = (0, \mu_0)$. The initial period of the zero-amplitude oscillation is

$$T_0 = \frac{2\pi}{w(0)}.$$

For a two variable system, the requirements that the eigenvalues are purely imaginary are $\mathrm{tr}J = 0$ and $\det J > 0$, where $\mathrm{tr}J$ and $\det J$ represent the trace and determinant of the Jacobian matrix (J) evaluated at the steady-state solution.

For a planar system there are three co-dimension one dynamic singularities. These are: the double-zero eigenvalue locus, also known as the Bogdanov–Takens bifurcation [13]; the double-Hopf locus, where two Hopf points come together; and the generalised (or degenerate) Hopf bifurcation, also known as a Bautin bifurcation [13], where a 'soft' Hopf bifurcation changes into a 'hard' Hopf bifurcation one (or vice versa); that is, when the first Lyapunov coefficient vanishes. The conditions for these are [14]:

Double-zero eigenvalue

$$f = g = \det J = \mathrm{tr}J = 0,$$
$$\frac{d}{d\lambda}\mathrm{tr}J \neq 0, \quad \mu_2 \neq 0, \quad \frac{d^2\lambda}{dx^2} \neq 0 \quad \text{and} \quad \frac{d^2\lambda}{dx^2} \neq \infty;$$

Double-Hopf locus

$$f = g = \mathrm{tr}J = \frac{d}{d\lambda}\mathrm{tr}J = 0, \qquad \frac{d^2\lambda}{dx^2} \neq 0, \quad \mu_2 \neq 0;$$

Generalised Hopf bifurcation

$$f = g = \mathrm{tr}J = \mu_1 = 0, \qquad \frac{d}{d\lambda}\mathrm{tr}J \neq 0, \quad \mu_2 \neq 0,$$

where μ_i is the ith Lyapunov coefficient of a Hopf point.

We shall not be concerned with the distinction between 'soft' and 'hard' Hopf bifurcations and do not consider the generalised Hopf bifurcation. We study the double-zero eigenvalue and the double-Hopf locus.

The Jacobian matrix for Eqs. (8–9) is

$$J = \begin{pmatrix} -\frac{1}{\tau} - \beta_1 & -\alpha_1 \\ \beta_1 & -\frac{1}{\tau} + \alpha_1 - \frac{\kappa_2}{[1+\rho\beta_1]^2} \end{pmatrix}. \tag{38}$$

Using Eq. (10) we obtain

$$\begin{aligned} \mathrm{tr}J = & \frac{(\alpha_1 - \kappa_2)\,{\alpha_1}^3\tau^3 - [1 + \alpha_1 - 2\rho\alpha_1\,(1-\alpha_1)]\,{\alpha_1}^2\tau^2}{\tau\alpha_1\,[\alpha_1\tau + \rho\,(1-\alpha_1)]^2} \\ & \frac{-\rho\,(1-\alpha_1)\,\alpha_1\,[2(1+\alpha_1) - \rho\alpha_1\,(1-\alpha_1)]\,\tau - \rho^2\,(\alpha_1+1)\,(1-\alpha_1)^2}{\tau\alpha_1\,[\alpha_1\tau + \rho\,(1-\alpha_1)]^2}, \end{aligned} \tag{39}$$

$$\begin{aligned} \det J = & \frac{-\left({\alpha_1}^2 - \kappa_2\right){\alpha_1}^2\tau^3 + [1 - 2\rho\alpha_1\,(1-\alpha_1)]\,{\alpha_1}^2\tau^2}{\alpha_1\tau^2\,[\alpha_1\tau + \rho\,(1-\alpha_1)]^2} \\ & \frac{+\rho\,(1-\alpha_1)\,\alpha_1\,[2 - \rho\alpha_1\,(1-\alpha_1)]\,\tau + \rho^2\,(1-\alpha_1)^2}{\alpha_1\tau^2\,[\alpha_1\tau + \rho\,(1-\alpha_1)]^2}. \end{aligned} \tag{40}$$

Expressions for the trace and determinant of the Jacobian were first obtained in [7, equation 28].

4.2 Double-zero eigenvalue

In this section we parameterise the double-zero eigenvalue bifurcation. We show that this bifurcation can not occur if the value of the saturation constant (ρ) is sufficiently low.

Using the singularity equation (11) and the defining conditions (39) and (40), we find that the double zero eigenvalue bifurcation curve is parameterised by

$$\tau = \frac{1}{{\alpha_1}^2\,(1-\alpha_1)}, \tag{41}$$

$$\beta_0 = (1-\alpha_1)^2\left[\rho{\alpha_1}^3\,(1-\alpha_1) - 1\right], \tag{42}$$

$$\kappa_2 = \left[(1-\alpha_1)^2\,\rho\alpha_1 + 1\right]^2\,{\alpha_1}^3. \tag{43}$$

Equation (42) can be rewritten in the form

$$\frac{(1-\alpha_1)^3\,\alpha_1^3}{(1-\alpha_1)^2 + \beta_0} = \frac{1}{\rho} \tag{44}$$

The left-hand side of Eq. (44) is a continuous function of the state variable on the closed region $0 \le \alpha_1 \le 1$. It therefore obtains a maximum value. It follows that there is a critical value of the saturation constant, $\rho_{\mathrm{cr}}\,(\beta_0)$, such that for $\rho < \rho_{\mathrm{cr}}\,(\beta_0)$ the

double zero eigenvalue bifurcation does not occur. An elementary bound on the critical value of ρ can be obtained as follows.

$$\frac{(1-\alpha_1)^3\,\alpha_1^3}{(1-\alpha_1)^2+\beta_0} < \frac{(1-\alpha_1)^3\,\alpha_1^3}{\beta_0} \leq \frac{1}{2^4\beta_0}.$$

This shows that there is no double-zero eigenvalue bifurcation when

$$\rho \leq 2^4\beta_0.$$

It follows that

$$\rho_{\rm cr}\,(\beta_0) > 2^4\beta_0.$$

For the case $\beta_0 = 0$ the maximum value of the RHS of Eq. (44) occurs when $\alpha_1 = 3^3/4^4$. It follows that

$$\rho_{\rm cr}\,(\beta_0 = 0) = \frac{4^4}{3^3} \approx 9.48.$$

It is useful to know when the double-zero eigenvalue curve intersects the line $\beta_0 = 0$. From Eqs. (42) and (43) we find that this happens when

$$\rho(\beta_0 = 0) = \frac{1}{(1-\alpha_1)\,{\alpha_1}^3}, \tag{45}$$

$$\kappa_2(\beta_0 = 0) = \frac{\left(1-\alpha_1+{\alpha_1}^2\right)^2}{\alpha_1}. \tag{46}$$

When $\rho = 10$ the physically meaningful solutions of Eq. (45) are $\alpha_{1,1} = 0.6753$ and $\alpha_{1,2} = 0.8159$. The corresponding values for the decay parameter are $\kappa_{2,1} = 0.9026$ and $\kappa_{2,1} = 0.8851$.

The double zero eigenvalue curve is shown in Fig. 4 for the case $\rho = 10$.

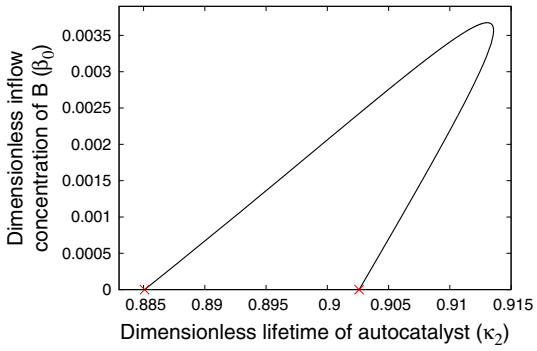

Fig. 4 The double-zero bifurcation curve in the secondary bifurcation parameter plane. Parameter value $\rho = 10$. The *red crosses* denote the crossing points $(\kappa_2, \beta_0) = (0.8851, 0)$ and $(\kappa_2, \beta_0) = (0.9026, 0)$ (Color figure online)

4.3 Double-Hopf locus

Differentiating the trace of the Jacobian with respect to the residence time τ we obtain

$$\frac{d\mathrm{tr}J}{d\tau} = \frac{2}{\tau^2} + \frac{(1+\rho\beta_1)^2(1-\alpha_1)}{\tau A_1} - \frac{A_2}{(1+\rho\beta_1)\tau A_3} + \frac{A_4}{A_1}, \tag{47}$$

where the coefficients A_i are

$$\begin{aligned}
A_4 &= \alpha_1\left[\alpha_1 + \rho\beta_1(\beta_1+\alpha_1-1-\beta_0)(\rho\beta_1+2) - \beta_0 - 1 + \beta_1 - \kappa_2\right] + \kappa_2,\\
A_3 &= \rho\beta_1\left[1+\tau(\beta_1-\alpha_1)\right](\rho\beta_1+2) + \tau\left[(\kappa_2\tau+1)\beta_1 - \alpha_1 + \kappa_2\right] + 1,\\
A_2 &= \left[(1+\rho\beta_1)^3 - 2\kappa_2\rho\right]\left[\beta_1(1+\tau(\beta_1+\alpha_1-1-\beta_0)) - \beta_0\right],\\
A_1 &= \tau\alpha_1(1+\rho\beta_1)^2 - (1+\beta_1\tau)\left[(1+\rho\beta_1)^2 + \kappa_2\tau\right].
\end{aligned}$$

Using Maple to solve the system (8)–(9), (39) and (47) gives a parameterisation of the double-Hopf curve. This parameterisation is too lengthy to include here.

Prior to plotting the double-Hopf locus it is informative to find its intersections with the line $\beta_0 = 0$. Using the parameterisation we find that, there are four such points: $\kappa_{2,1} = 0.1128$, $\kappa_{2,2} = 0.9043$, $\kappa_{2,3} = 0.8794$ and $\kappa_{2,4} = 0.8881$. The value $\kappa_{2,2} \approx 0.941$ was identified earlier using path-following methods [9, p. 485].

Figure 5 shows the locus of the double Hopf bifurcation points. The part of the locus connecting the points $(\kappa_2, \beta_0) = (0.8794, 0)$ and $(\kappa_2, \beta_0) = (0.8881, 0)$ is too small to be seen in the Fig. 5a, it is shown in Fig. 5b.

A close comparison of the double-zero eigenvalue and double-zero Hopf curves reveals that for some points in region B it is possible trace a curve that ultimately enters into the small region shown in Fig. 5b without crossing the double-zero eigenvalue locus. This indicates that a steady-state diagram corresponding to values of the secondary bifurcation parameters inside this small region must have either zero or

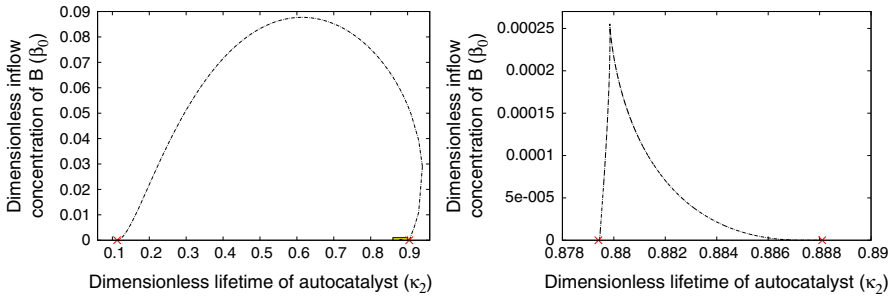

Fig. 5 The double-Hopf point bifurcation curve in the secondary birucation parameter plane. Parameter value: $\rho = 10$. The *red crosses* denote the crossing points $(\kappa_2, \beta_0) = (0.1128, 0)$ and $(0.9043, 0)$, in **a**, and $(\kappa_2, \beta_0) = (0.8794, 0)$ and $(0.8881, 0)$, in **b**. The *small yellow rectangle* in **a** is shown in **b** (Color figure online)

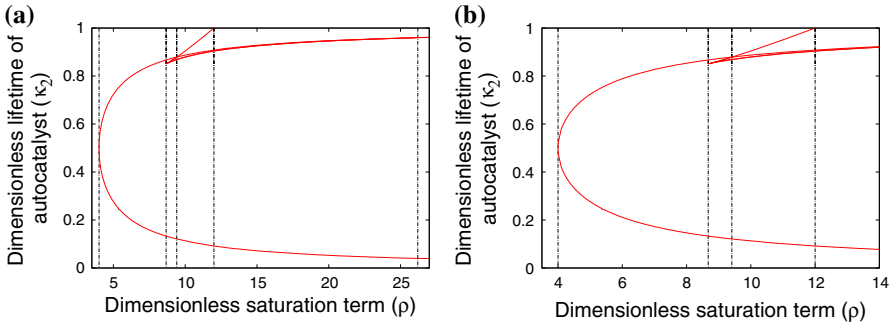

Fig. 6 The locus of the points on the double Hopf singularity for which $\beta_0 = 0$. As explained in the text, there are two critical value for the unfolding parameter ρ: $\rho_{\mathrm{cr},1} = 8.763$ and $\rho_{\mathrm{cr},2} = 4$

four Hopf bifurcation points. Construction of a steady-state diagram shows that it is the latter.

Figure 6 shows the locus of the intersection points along the line $\beta_0 = 0$ as a function of the saturation constant. This reveals that there are two critical values of the saturation constant. At the first critical value, $\rho_{\mathrm{cr},1}$ the number of intersection points changes from four to two, below this value steady-state diagrams no longer contain four Hopf bifurcation points. At the second critical value, $\rho_{\mathrm{cr},2}$, the number of intersection points changes from two to zero. As noted in [9, p. 472] below this value the double-Hopf curve is no longer physically meaningful.

We use our parameterisation of the double-Hopf curve to show that these critical values occur when $\rho_{\mathrm{cr},1} = 8.67$ and $\rho_{\mathrm{cr},2} = 4.0$. The former was previously identified in [9] through the use of path-following methods. When $\beta_0 = 0$ we can simplify the parametric representation of the double-Hopf locus to show that the intersection points occur when either

$$\rho\alpha_1^2 - \rho\alpha + 1 = 0 \tag{48}$$

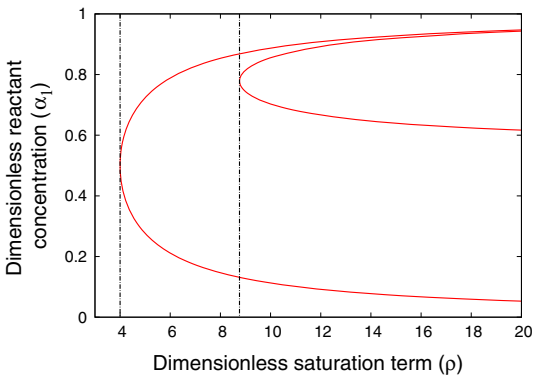

Fig. 7 The double-Hopf locus along the plane $\beta_0 = 0$. The critical values for the saturation constant are: $\rho_{\mathrm{cr},1} = 4$ and $\rho_{\mathrm{cr},2} = 8.763$

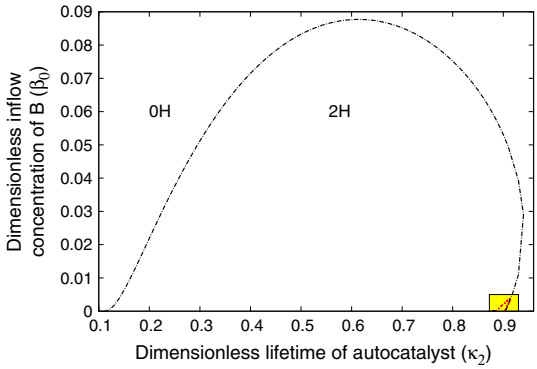

Fig. 8 The combined degenerate Hopf bifurcation diagram comprising the double zero eigenvalue curve (*red*) and the double Hopf locus (*black*). The number of Hopf bifurcation points on the steady-state diagram is indicated. The *yellow region* is blown-up in Fig. 9. Parameter value: $\rho = 10$ (Color figure online)

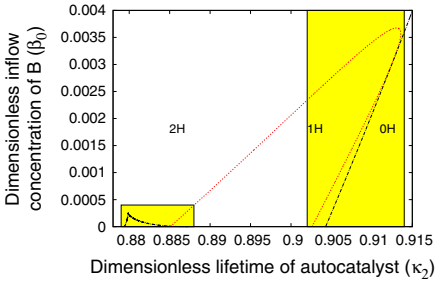

(a) Blow-up of figure 8 (a).

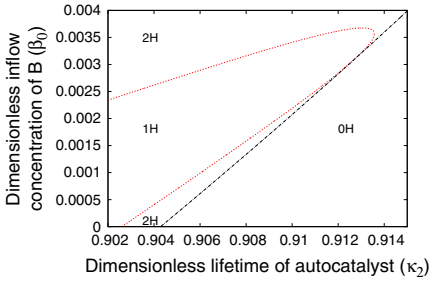

(b) Blow-up of figure 9 (a)

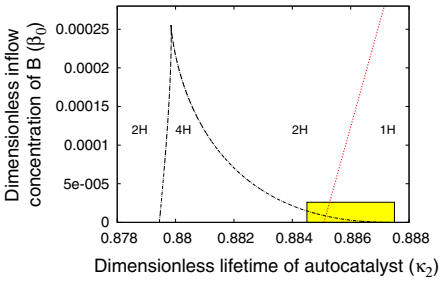

(c) Blow-up of figure 9 (a)

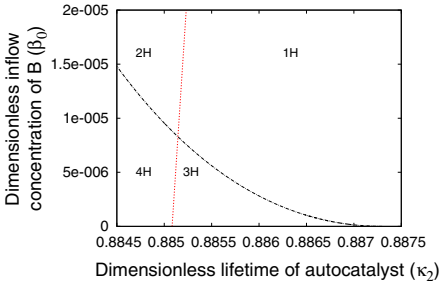

(d) Blow-up of figure 9 (c).

Fig. 9 The degenerate Hopf bifurcation diagram: and double zero eigenvalue bifurcation (*red*) and double-Hopf locus (*black*). Parameter value: $\rho = 10$ (Color figure online)

or

$$G = -\rho{\alpha_1}^3 - (1+2\rho)\,{\alpha_1}^2 + (5\rho+1)\,\alpha_1 - 2\,(1+\rho) = 0. \tag{49}$$

From Eq. (48) we find that

$$\alpha_1 = \frac{\rho \pm \sqrt{\rho(\rho-4)}}{2\rho}. \tag{50}$$

This gives the critical value $\rho_{\mathrm{cr},2} = 4$.

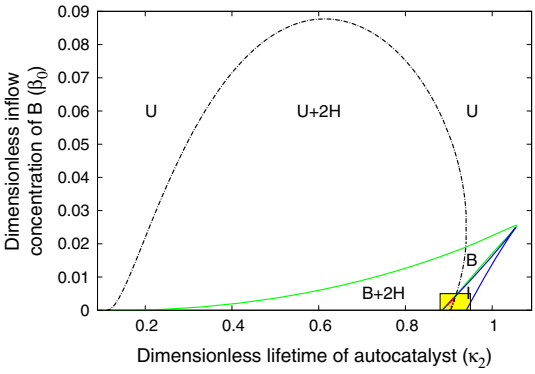

Fig. 10 The combined bifurcation diagram: cusp curve (*green*), double-Hopf locus (*black*), double zero eigenvalue curve (*red*) and isola curve (*blue*). B: breaking wave, B+2H: breaking wave with two Hopf bifurcation points, I: isola and U: unique, U+2H: unique with two Hopf bifurcation points. The *yellow rectangle* is blown-up in Fig. 11. Parameter value: $\rho = 10$ (Color figure online)

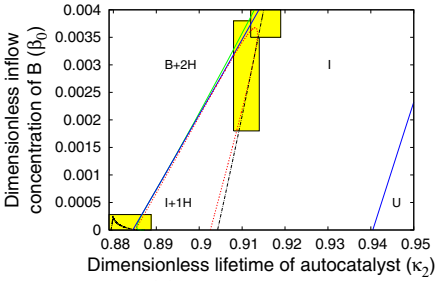

(a) Blow-up of figure 10.

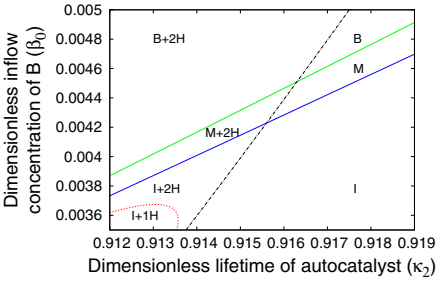

(b) Blow-up of figure 11 (a).

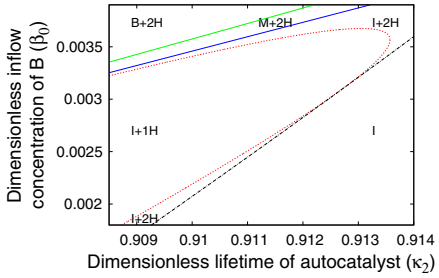

(c) Blow-up of figure 11 (a).

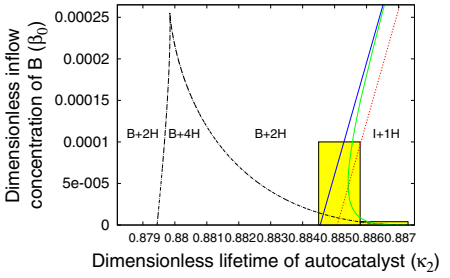

(d) Blow-up of figure 11 (a).

Fig. 11 The combined bifurcation diagram: cusp curve (*green*), double-Hopf locus (*black*), double-zero eigenvalue curve (*red*) and isola curve (*blue*). B: breaking wave, B+2H: breaking wave with two Hopf points, B+4H: breaking wave with four Hopf points, I: isola, I+1H: isola with one Hopf point, I+B+2H: isola with breaking wave and two Hopf bifurcation points, M: mushroom and U: unique, U+2H: unique with two Hopf points. Parameter value: $\rho = 10$ (Color figure online)

To find the second critical value we observe that Fig. 7 shows that this is a limit-point bifurcation on the implicit curve defined by the singularity curve (49). A limit point bifurcation occurs when $G = \frac{dG}{d\alpha_1} = 0$ and the non-degeneracy conditions $\frac{d^2G}{d{\alpha_1}^2} \neq 0$ and $\frac{dG}{d\rho} \neq 0$ are satisfied. Solving $G_{\alpha_1} = 0$ for ρ we obtain that

$$\rho = \frac{1 - 2\alpha_1}{3{\alpha_1}^2 + 4\alpha_1 - 5}. \tag{51}$$

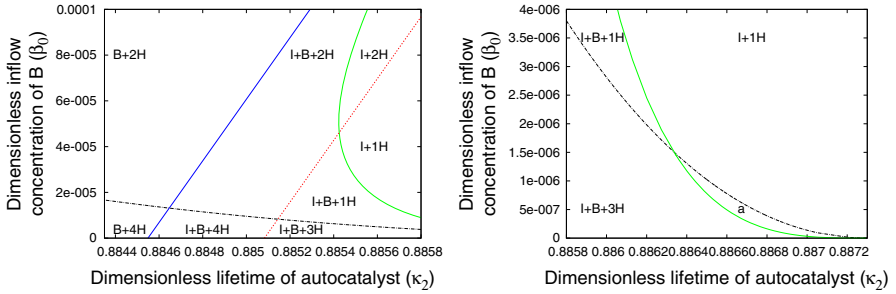

(a) Blow-up of figure 11 (d) **(b)** Blow-up of figure 11 (d)

Fig. 12 The combined bifurcation diagram: cusp curve (*green*), double Hopf bifurcation dash curve (*black*), double zero curve (*red*) and isola curve (*blue*). B+2H: breaking wave with double Hopf points, B+4H: breaking wave with four Hopf points, I+B+2H: isola with breaking wave and two Hopf points, I+1H: isola with one Hopf point, I+2H: isola with two Hopf points, a: isola with three Hopf points, I+B+1H: isola with breaking wave and one Hopf points, I+B+3H: isola with breaking wave and three Hopf points and I+B+4H: isola with breaking wave and four Hopf points. Parameter value: $\rho = 10$ (Color figure online)

Substituting (51) into the singularity equation (49) we have

$$G = -\frac{(\alpha_1 + 1)\left({\alpha_1}^3 - 3{\alpha_1}^2 + 12\alpha_1 - 8\right)}{3{\alpha_1}^2 + 4\alpha_1 - 5} = 0. \tag{52}$$

The only physically meaningful solution of the system (51) and (52) is $(\rho, \alpha_1) = (8.763, 0.779)$. Direct calculation shows that the non-degeneracy conditions are satisfied at this point. Thus the second critical value is $\rho_{\mathrm{cr},1} = 8.763$.

Table 3 Tabulation of the generic steady-state diagrams

	Bifurcation figure							SSD
	10	11 (a)	11 (b)	11 (c)	11 (d)	12 (a)	12 (b)	
B	√		√					Fig. 13a
B+2H	√	√	√	√	√	√		Fig. 13b
B+4H					√	√		Fig. 13c
I	√	√	√	√				Fig. 14a
I+1H		√	√	√	√	√	√	Fig. 14b
I+2H			√	√		√		Fig. 14c
I+3H							√	Fig. 15a, b
I+B+1H						√		Fig. 16a
I+B+2H						√	√	Fig. 16b
I+B+3H						√	√	Fig. 17
I+B+4H						√		Fig. 18a, b
M			√					Fig. 19a
M+2H			√	√				Fig. 19b
U	√	√						Fig. 20a
U+2H	√							Fig. 20b, c

SSD steady-state diagram

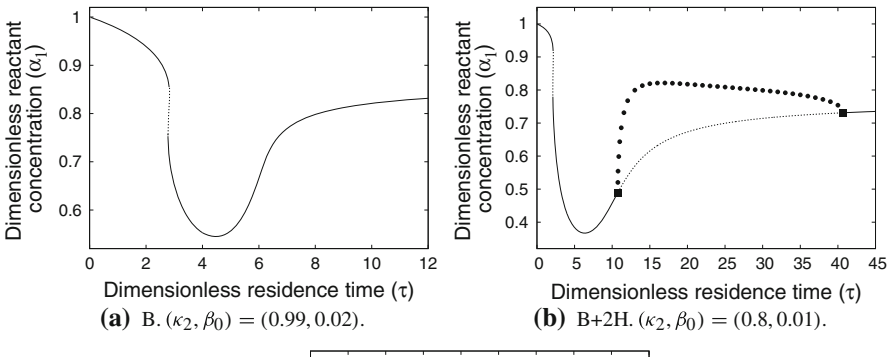

(a) B. $(\kappa_2, \beta_0) = (0.99, 0.02)$. **(b)** B+2H. $(\kappa_2, \beta_0) = (0.8, 0.01)$.

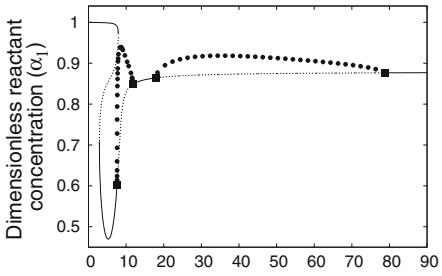

(c) B+4H. $(\kappa_2, \beta_0) = (0.88, 0.0001)$

Fig. 13 The three generic 'breaking wave' steady-state diagrams. Parameter value: $\rho = 10$

We conclude that along the double-Hopf locus there are two critical values for the saturation constant. There are $\rho_{\mathrm{cr},1} = 4$ and $\rho_{\mathrm{cr},2} = 8.763$. The former value was identified in [9, p. 472].

4.4 Double zero eigenvalue and double Hopf bifurcation diagram

In this section we combine the double-zero eigenvalue curve from Sect. 4.2 with the double-Hopf curve from Sect. 4.3. The combined degenerate Hopf bifurcation curve is shown in Fig. 8. This curve splits the secondary bifurcation plane into distinct regions. Crossing from one region to an adjacent region changes the number of Hopf bifurcations on the steady-state diagram. The number of Hopf bifurcations in each region is indicated in the figure.

Figure 9 shows a blow-up of the very small region in Fig. 8 (indicated in yellow) where there are steady-state diagrams with one, two, three or four Hopf bifurcation points.

5 Putting it all together

In this section we combine the static and dynamic multiplicity analysis from Sects. 3.2.4 and 4.4 to classify all possible steady-state diagrams. Figure 10 shows the

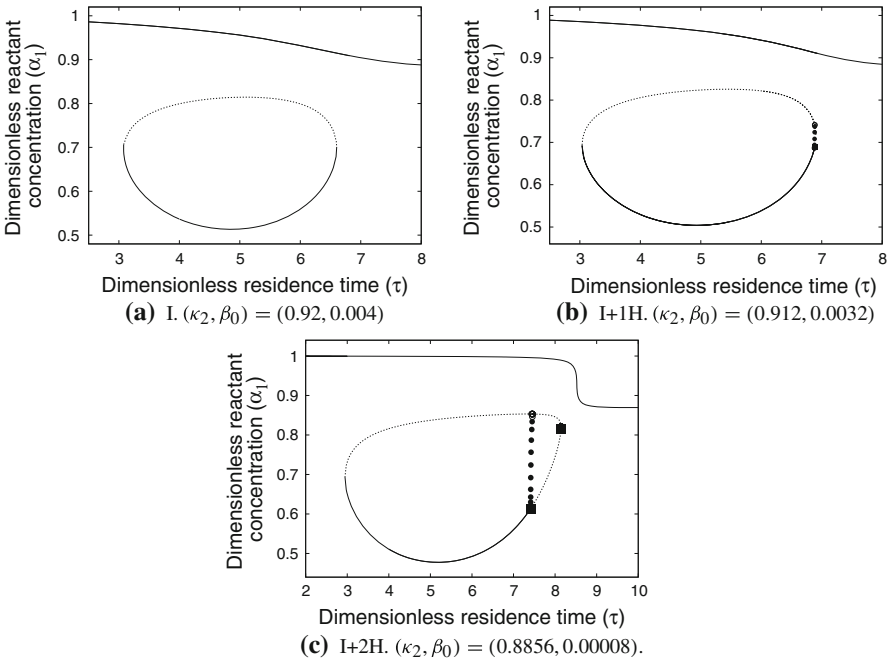

Fig. 14 Three generic 'isola' steady-state diagrams. In **b** and **c** all periodic solutions are terminated by homoclinic bifurcations. Parameter value: $\rho = 10$

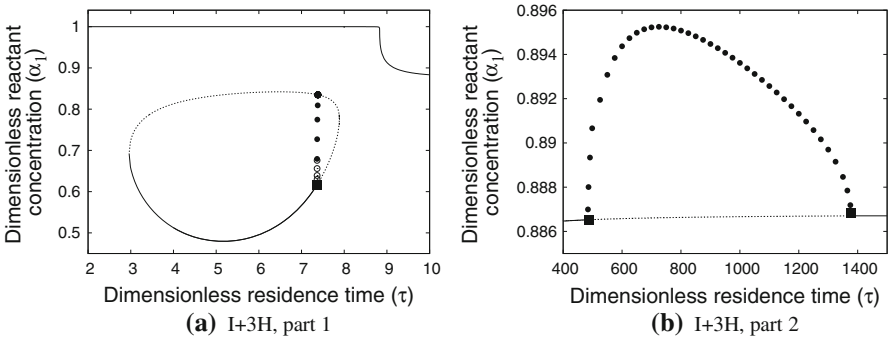

Fig. 15 The fourth generic 'isola' steady-state diagram. Parameter value: $\rho = 10$; $(\kappa_2, \beta_0) = (0.8868, 0.0000003)$

resulting bifurcation diagram in the secondary parameter plane. Some of the steady-state diagrams occur within the very small parameter region indicated in yellow. These are shown in Fig. 11. In turn, two small regions in Fig. 11 are blown-up in Fig. 12.

In these figures the 'type' of the steady-state diagram is indicated. This classification has two components. The first indicates the underlying steady-state diagram (U, B, M, I and B + I) whilst the second indicates the number of Hopf bifurcation points (0, 1, 2, 3 and 4). If the number of Hopf points is absent, e.g., 'U', then the number is zero.

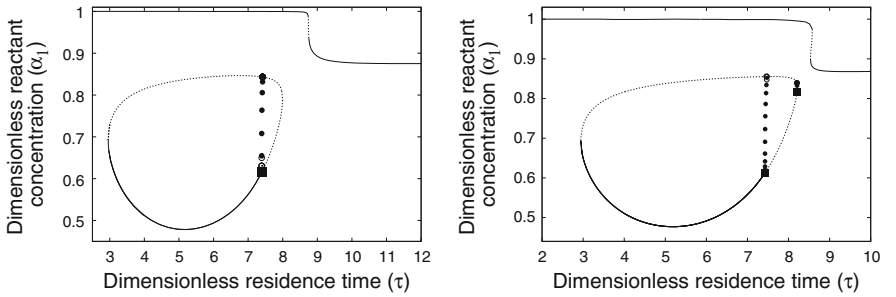

(a) I+B+1H. $(\kappa_2, \beta_0) = (0.886, 0.0000035)$ **(b)** I+B+2H. $(\kappa_2, \beta_0) = (0.885, 0.000025)$

Fig. 16 Two generic 'isola with breaking wave' steady-state diagrams. Parameter value: $\rho = 10$

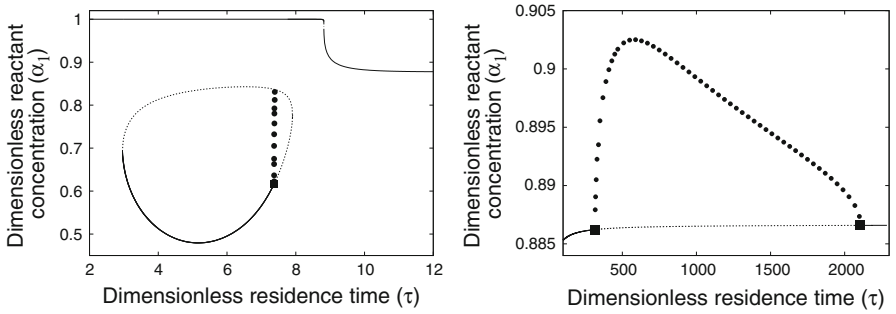

(a) I+B+3H, part 1 **(b)** I+B+3H, part 2

Fig. 17 The third generic 'isola with breaking wave' steady-state diagram. Parameter value: $\rho = 10$, $(\kappa_2, \beta_0) = (0.88665, 0.0000003)$

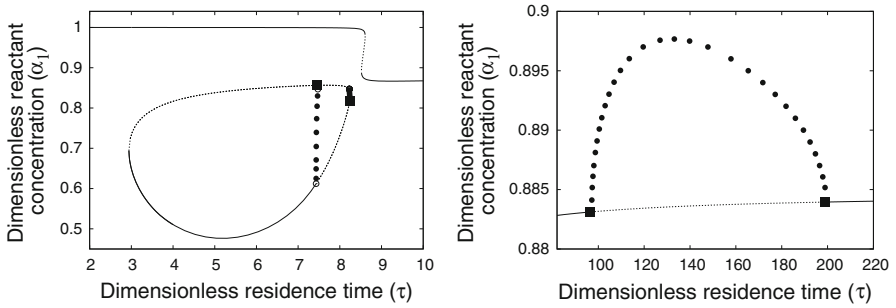

(a) I+B+4H, part 1 **(b)** I+B+4H, part 2

Fig. 18 The fourth generic 'isola with breaking wave' steady-state diagrams. Parameter value: $\rho = 10$, $(\kappa_2, \beta_0) = (0.8848, 0.00001)$

Table 3 tabulates the generic steady-state diagrams, indicating upon which bifurcation diagram they are located and the figure in which the steady-state diagram is shown.

Figure 13 shows the breaking wave steady-state diagrams, Figs. 14 and 15 the isola steady-state diagrams, Figs. 16, 17 and 18 the isola with breaking wave steady-state

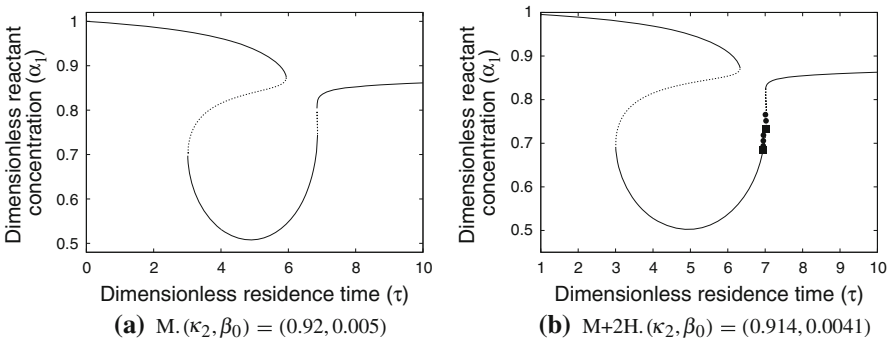

(a) M. $(\kappa_2, \beta_0) = (0.92, 0.005)$ **(b)** M+2H. $(\kappa_2, \beta_0) = (0.914, 0.0041)$

Fig. 19 The two generic 'mushroom' steady-state diagrams. In (b) the periodic solutions are terminated at homoclinic bifurcations. Parameter value: $\rho = 10$

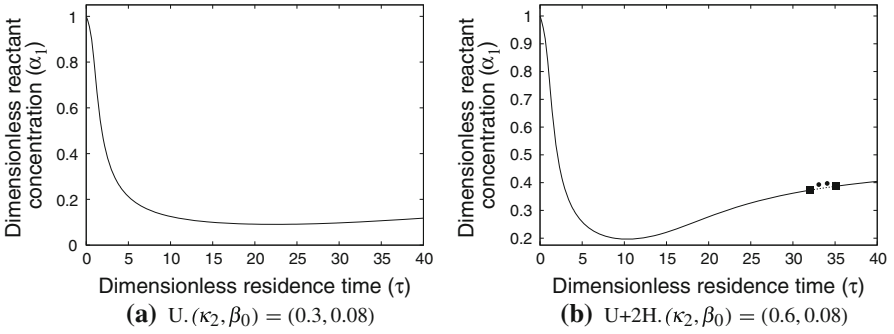

(a) U. $(\kappa_2, \beta_0) = (0.3, 0.08)$ **(b)** U+2H. $(\kappa_2, \beta_0) = (0.6, 0.08)$

Fig. 20 The two generic 'unique' steady-state diagrams. Parameter value: $\rho = 10$

diagrams, Fig. 19 the mushroom steady-state diagrams and Fig. 20 the unique steady-state diagrams.

In Fig. 14c the periodic solutions generated by the Hopf bifurcation point when $\tau = 8.14$ are not visible on the figure. In Fig. 15 one Hopf bifurcation point is on the isola and two are in the 'main' curve. The latter at large values of the residence time respectively.

In Fig. 16 all the Hopf bifurcation points are on the isola. However, in Fig. 17 there one Hopf bifurcation point on the isola and two on the breaking wave. The latter occur when the residence time is very large and the steady-state diagram is split into two parts: for small and large values of the residence time respectively.

6 Conclusions

We have investigated the behaviour of quadratic autocatalyst subject to a non-linear decay term exhibiting a saturation effect in a continuously stirred tank reactor. Aspects of this model have previously been studied by a combination of analytic [7,8] and path-following [9] techniques.

The contribution of our work is to re-analyse this model using the techniques of singularity theory and degenerate Hopf bifurcation theory. By providing analytical representations for the cusp, isola, double zero, and double Hopf point singularities we are able to generate the bifurcation diagram without the use of path-following methods. (Such methods are still required to generate the steady-state diagrams). These representations provide extra insight into the behaviour of the model as the saturation constant is varied. In particular, we found critical values for the saturation constant at which the first three of these curves disappeared. For the double-Hopf curve we found critical values for the special case when $\beta_0 = 0$. These results provide general criteria for static multiplicity and periodic solutions.

We used the bifurcation diagram to generate all steady-state diagrams, modulo the distinction between sub- and super-critical Hopf bifurcations. Some of these steady-state diagrams exist in very small parameter regions, which would be difficult to find without the use of the techniques employed here. Only the cases U, B, B+2H, B+4H, I and M were previously known.

Appendix: Globally attracting invariant region

Here we show that the region

$$\begin{aligned} 0 \leq \alpha_1 \leq 1, \\ 0 \leq \beta_1 \leq 1 + \beta_0 \end{aligned}$$

is both (positively) invariant and exponentially attracting for any solution with physically meaningful initial conditions outside it.

We first demonstrate that solutions with non-negative initial conditions can not become negative. We have

$$\begin{aligned} \left.\frac{\mathrm{d}\alpha_1}{\mathrm{d}t}\right|_{\alpha_1=0} &= \frac{1}{\tau} > 0, \\ \left.\frac{\mathrm{d}\beta_1}{\mathrm{d}t}\right|_{\alpha_1=0} &= \frac{\beta_0}{\tau} \geq 0. \end{aligned}$$

(Observe that when $\beta_0 = 0$ that the line $\beta = 0$ is itself invariant).

We now show that solutions with (physically meaningful) initial conditions outside the region $0 \leq \alpha_1 \leq 1$ are exponentially attracted to it. From Eq. (8) we have

$$\begin{aligned} \frac{d\alpha_1}{dt^*} &= \frac{1-\alpha_1}{\tau} - \alpha_1\beta_1, \\ &\leq \frac{1-\alpha_1}{\tau} \quad \text{as } \alpha_1 \geq 0 \text{ and } \beta_1 \geq 0. \end{aligned}$$

It follows that

$$\alpha_1\left(t^*\right) \leq 1 - \left[1 - \alpha_1\left(0\right)\right] \exp\left[-\frac{t^*}{\tau}\right],$$

i.e. the solution trajectory is attracted into the invariant region. This inequality also demonstrates that the region $0 \leq \alpha_1 \leq 1$ is positively invariant.

We have shown that the reactant concentration (α_1) is bounded. We now show that the autocatalyst concentration (β_1) is bounded. Let $Z_1\left(t^*\right) = \alpha_1\left(t^*\right) + \beta_1\left(t^*\right)$ (As α_1 and β_1 are both non-negative so it Z_1.) Adding Eqs. (8) and (9) we have

$$\begin{aligned}\frac{\mathrm{d}Z}{\mathrm{d}t^*} &= \frac{1 + \beta_0 - Z_1}{\tau} - \frac{\kappa_2\beta_1}{1 + \rho\beta_1} \\ &\leq \frac{1 + \beta_0 - Z_1}{\tau}, \quad \text{as} \quad \beta_1(t^*) \geq 0.\end{aligned}$$

It follows that

$$Z\left(t^*\right) \leq 1 + \beta_0 - \left[1 + \beta_0 - \left(\alpha_1\left(0\right) + \beta_1\left(0\right)\right)\right] \exp\left[-\frac{t^*}{\tau}\right].$$

This inequality demonstrates that if the initial condition is within the invariant region $\left(1 + \beta_0 - \left(\alpha_1\left(0\right) + \beta_1\left(0\right)\right) > 0\right)$ then the corresponding solution remains in it for all time. Furthermore, if the initial condition is outside the invariant region $\left(1 + \beta_0 - \left(\alpha_1\left(0\right) + \beta_1\left(0\right)\right) < 0\right)$ then the solution is attracted into the invariant region exponentially quickly.
In the limit $t^* \to \infty$

$$\begin{aligned}Z\left(t^*\right) &\leq 1 + \beta_0 \\ \Rightarrow \alpha_1 + \beta_1 &\leq 1 + \beta_0.\end{aligned}$$

As the reactant α_1 is bounded so is the autocatalyst. The use of simple differential inequalities to establish solutions boundedness in these types of systems stems from [15] (though was possibly known much earlier).

References

1. P. Gray, S.K. Scott, *Chemical Oscillations and Instabilities: Non-linear Chemical Kinetics* (Oxford University Press, Oxford, 1990)
2. P. Gray, S.K. Scott, *Chemical Oscillations* (Oxford University Press, Oxford, 1990)
3. S.K. Scott, *Oscillations, Waves, and Chaos in Chemical Linetics, vol. 18 of Oxford Chemistry Primers* (Oxford University Press, Oxford, 1994)
4. K.F. Lin, Concentration multiplicity and stability for autocatalytic reactiona in a continuous stirred-tank reactor. Can. J. Chem. Eng. **57**, 476–480 (1979)
5. K.F. Lin, Multiplicity, stability and dynamics for isothermal autocatalytic reactions in CSTR. Chem. Eng. Sci. **36**(9), 1447–1452 (1981)
6. P. Gray, S.K. Scott, Autocatalytic reactions in the isothermal, continuous stirred tank reactor: Isolas and other forms of multistability. Chem. Eng. Sci. **38**, 29–43 (1983)

7. J.H. Merkin, D.J. Needham, S.K. Scott, A simple model for sustained oscillations in isothermal branched-chain or autocatalytic reactions in a well stirred open system. I. Stationary states and local stabilities. Proc. R. Soc. Lond. **398**, 81–100 (1985)
8. J.H. Merkin, D.J. Needham, S.K. Scott, A simple model for sustained oscillations in isothermal branched-chain or autocatalytic reactions in a well stirred open system. II. Limit cycles and non-stationary states. Proc. R. Soc. Lond. **398**, 101–116 (1985)
9. J. Brindley, C. Kaas-Petersen, J.H. Merkin, S.K. Scott, A simple model for sustained oscillations in isothermal branched-chain or autocatalytic reactions in a well-stirred open system. III. Multiple stationary states and Hopf bifurcations. Proc. R. Soc. Lond. **417**, 463–496 (1988)
10. A. Ajbar, K. Alhumaizi, *Dynamics of the Chemostat: A Bifurcation Theory Approach* (Taylor and Francis Ltd, London, 2012)
11. B.D. Hassard, N.D. Kazarinoff, Y.H. Wan, *Theory and Applications of Hopf Bifurcation* (Cambridge University Press, New York, 1981)
12. L.J.S. Allen, *An Introduction to Mathematical Biology* (Prentice Hall, Englewood Cliffs, 2007)
13. Y.A. Kuznetsov, *Elements of Applied Bifurcation Theory*, 1st edn. (Springer, Prentice Hall, New York, 1995)
14. B.F. Gray, M.J. Roberts, A method for the complete qualitative analysis of two coupled ordinary differential equations dependent on three parameters. Proc. R. Soc. Lond. **416**, 361–389 (1988)
15. S.B. Hsu, S.P. Hubbell, P. Waltman, Competing predators. SIAM J. Appl. Math. **35**(4), 617–625 (1978)